ELSEVIER

Thermochimica Acta 282/283 (1996) 81–90

thermochimica acta

A kinetic study of the thermal decomposition of iron(III) oxide-hydroxides.

Part 3. Shape control and thermal decomposition of α-FeO(OH)[1]

Nobuyoshi Koga [a,*], Shigeru Takemoto [a], Tatsuya Nakamura [b], Haruhiko Tanaka [a]

[a] *Chemistry Laboratory, Faculty of School Education, Hiroshima University, 1-1-1 Kagamiyama, Higashi-Hiroshima 739, Japan*

[b] *Research and Development Division, Toda Kogyo Corp., 4-1-2 Funairi-Minami, Naka-ku, Hiroshima 730, Japan*

Abstract

The shape control of crystalline particles of α-FeO(OH) was performed through growth treatment in an aqueous medium and subsequent hydrothermal treatment. The samples were subjected to a thermogravimetric (TG) study. The different TG curves obtained for the samples before and after the hydrothermal treatment were explained in connection with the existence of an irregular outer surface layer on the samples before the hydrothermal trreatment. The overall decomposition kinetics of the samples after hydrothermal treatment were determined by analyzing the TG curves at different heating rates. An apparent activation energy of approx. 140 kJ mol^{-1} was obtained in the restricted range of fractional reaction $0.4 \leq \alpha \leq 0.95$, irrespective of the samples. The appropriate kinetic model functions changed from nucleation growth to reaction interface shrinkage with increasing particle size. The correspondence of the overall kinetics obtained from the thermoanalytical method with the physico-geometry of the reaction is discussed briefly.

Keywords: α-FeO(OH); Kinetics; Shape control; TG; Thermal decomposition

* Corresponding author.

[1] Dedicated to Takeo Ozawa on the Occasion of his 65th Birthday.

SSDI 0040-6031(96)02824-9

1. Introduction

The present study discusses the relation between the morphology, the particle size and distribution of iron(III) oxide-hydroxides and the kinetics of thermal decompositions [1, 2], motivated by their practical importance as an objective material and as a precursor of iron(III) oxides. The correspondence of the overall kinetic results obtained from a thermoanalytical (TA) study with the physico-geometry of the actual decomposition of the respective crystalline particles is also discussed in the present study, because of difficulties encountered in providing a satisfactory kinetic description by combining macroscopically-averaged TA data and mathematically-simplified physico-geometric kinetic models originally derived from microscopically-based observations [3–6]. Later, we studied the relation between the thermal decomposition kinetics of γ-FeO(OH) and the shape and size of the crystalline particles prepared through an oxidative hydrolysis of iron(II) chloride solution using a urea decomposition [2]. On changing the shape and size of the particles, a systematic change in the appropriate kinetic model was observed for both the isothermal and nonisothermal decompositions.

It was reported by Kiyama et al. [7] that the size of the needle-like α-FeO(OH) crystals is controlled by changing the conditions through air oxidation of aqueous suspensions containing iron(II) precipitates. Recently, the shape control of α-FeO(OH) crystalline particles was performed through growth treatment of seed crystals in an aqueous medium and consequent hydrothermal treatment [8, 9]. Here we deal with the kinetics of the thermal decomposition of α-FeO(OH) crystalline particles with different sizes and shapes prepared as reported by Asai et al. [9]. Systematic kinetic analyses of the thermogravimetric (TG) curves were made employing the method of kinetic analysis described earlier [1, 2, 4, 10].

2. Experimental

2.1. Sample preparation

To prepare 600 ml of the dilute solution, 9.3 g of regent grade $FeSO_4 \cdot 7H_2O$ and 33.0 g of KOH were dissolved in distilled water. The solution was stirred mechanically for 6 days at 50°C. The precipitate obtained by air oxidation was used as the seed particles for further control of the particle morphology.

$FeSO_4 \cdot 7H_2O$ (5.0 g) was dissolved in 80 ml of distilled water. After adding 2 ml of 0.1 M H_2SO_4 to avoid hydrolysis, the solution was diluted with distilled water to 250 ml to provide the solution for crystal growth. Adding an iron wire the solution as a source of Fe^{2+}, 5.0 g of the seed particles were dispersed in the mother solution by introducing air at a rate of 20 ml min^{-1} to grow the particles over a number of days. The precipitates were filtered and washed with distilled water and dried at 60°C for 20 h.

By dispersing 1.0 g of the particles into 45 ml of NaOH solution, the hydrothermal treatment was performed in 100-ml vessels for 3 h at 200°C. The resultant particles were filtered and washed by distilled water and dried at 60°C for 20 h.

2.2. Measurements

The precipitated phases in the respective steps of sample preparation were characterized by X-ray powder diffractometry (Rigaku-miniflex, Mn-filtered Fe Kα) and FT-IR spectroscopy (Shimadzu FT-IR 8100, diffuse reflectance method). The specific surface area of the samples was measured using the BET method. The particle size and shape of the samples were observed by transmission electron microscopy (JEOL, JEM-100S) after pouring an aqueous suspension of the sample powder onto a carbon mesh on a copper grid.

3.0 mg of the sample was weighed onto a platinum crucible, 2.5 mm in height and 5 mm in diameter. TG traces were recorded using a Shimadzu TGA-50 at various heating rates ϕ, $0.5 \leq \phi \leq 10.0$ K min^{-1}, under flowing N_2 at a rate of 30 ml min^{-1}.

3. Results and discussion

3.1. Shape control

The precipitates obtained at the respective stages of the preparation were identified as α-FeO(OH) by XRD and FT-IR. Fig. 1 shows the change in the specific surface area depending on the growth treatment time. Although the specific surface area increases on initial crystal growth, a rapid decrease in the specific surface area is observed between 8 and 24 days. For longer growth treatments, change in the specific surface area is not apparent. After the hydrothermal treatment, the specific surface area decreases irrespective of the growth treatment time.

Fig. 2 reproduces typical TEM photographs of the particles after the growth and hydrothermal treatments. It is apparent that during the growth treatment the needle-

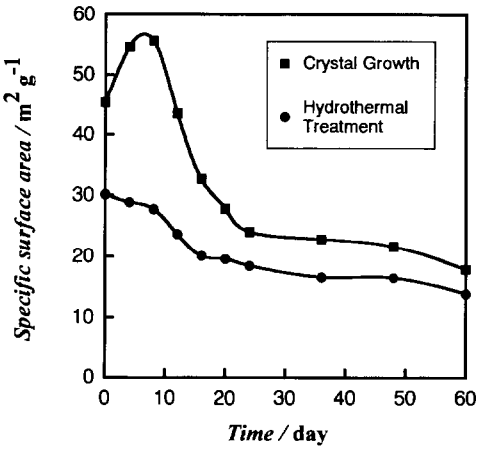

Fig. 1. Change in the specific surface area depending on the growth treatment time.

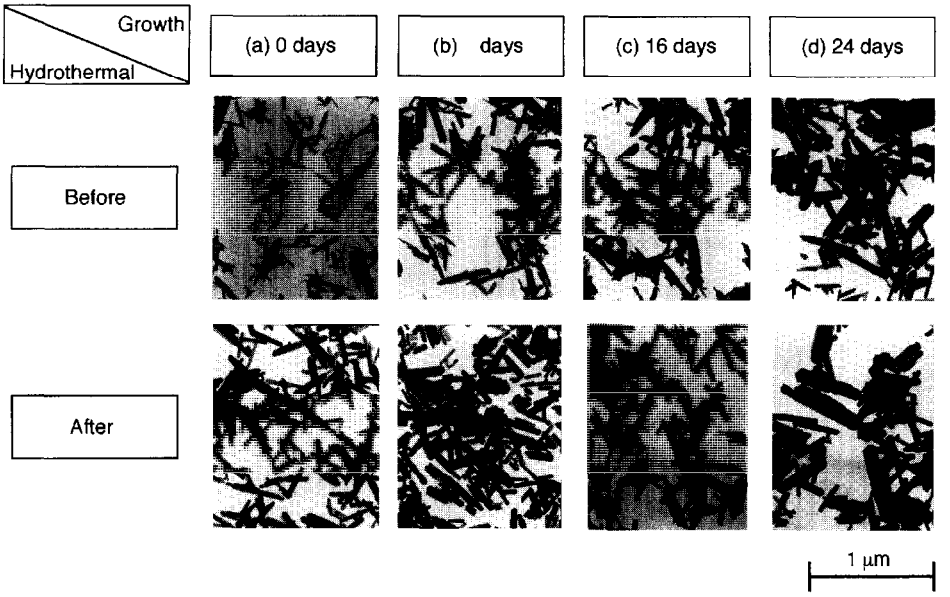

Fig. 2. Typical TEM photographs of the samples after growth and hydrothermal treatments.

like particles grow with a slightly decreasing aspect ratio [9]. The particles before hydrothermal treatment exhibit irregularity at the growth boundary on the surfaces. The irregular layer on the surface dissolves and is recrystallized as smooth surfaces during the hydrothermal treatment. This may be one of the reasons for the decrease in the specific surface area during hydrothermal treatment [9]. A comparison of the TG-DTG curves for the thermal decomposition of α-FeO(OH) to α-Fe_2O_3 before and after hydrothermal treatment is shown in Fig. 3. Two clear peaks are observed in the DTG curve for the sample before hydrothermal treatment. The samples after hydrothermal treatment give only one peak corresponding to the second peak of the sample before hydrothermal treatment. It seems that the first peak of the sample before hydrothermal treatment corresponds to the thermal decomposition of the irregular layer on the surface.

3.2. *Decomposition kinetics*

The thermal decomposition of the samples after hydrothermal treatment was subjected to kinetic study, because of the single-step reaction. Fig. 4 shows plots of fractional reaction α against temperature T for the thermal decomposition of the samples after hydrothermal treatment, together with their derivative curves. The peak maxima of the derivative curves shift towards the lower temperatures with increasing particle size. This apparently indicates the opposite tendency of the effect of particle size

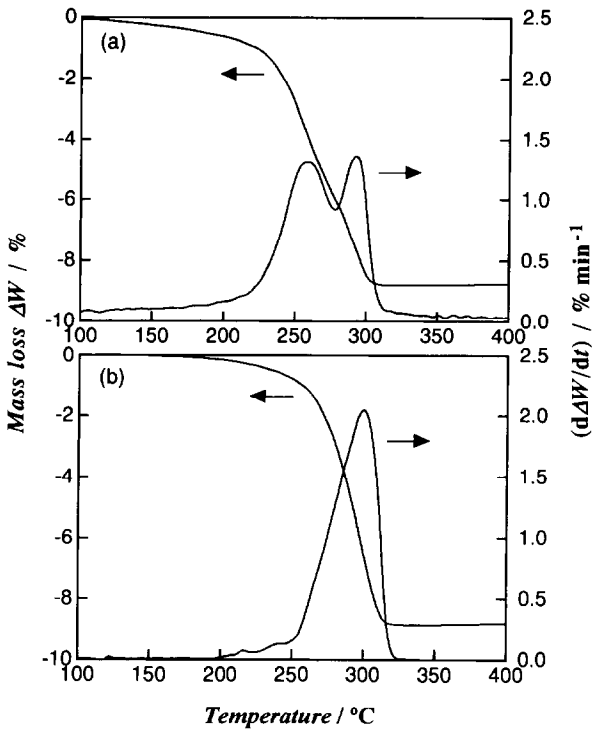

Fig. 3. TG–DTG curves for the thermal decomposition of the samples grown for 16 days ($\phi = 10$ K min^{-1}): (a) before the hydrothermal treatment; (b) after the hydrothermal treatment.

on TA curves of the solid-state transformation governed by a reaction interface shrinkage mechanism.

On the basis of the plots of $d\alpha/dt$ against T at various heating rates ϕ, $0.5 \leq \phi \leq 10.0$ K min^{-1}, the apparent activation energies E at various α were calculated by plotting $\ln(d\alpha/dt)$ against T^{-1} according to the Friedman method [11]

$$\ln\left(\frac{d\alpha}{dt}\right) = \ln[Af(\alpha)] - \frac{E}{RT} \tag{1}$$

where A, $f(\alpha)$ and R are the preexponential factor, kinetic model function and gas constant, respectively. Fig. 5 represents the α dependence of the apparent E. Fluctuation in the values of E was observed for the early part of the reaction, particularly for the sample of the smallest particle size. This may be due to the particle size distribution and to the residual part of the irregular surface layer. The nearly constant E values were obtained in the restricted range of $0.4 \leq \alpha \leq 0.95$. In this region, the value of E is practically the same irrespective of the different particle size of the samples.

The rate data in the restricted range $0.4 \leq \alpha \leq 0.95$ were subjected to further kinetic analysis, because of the constant E irrespective of α satisfying the prerequisite of the

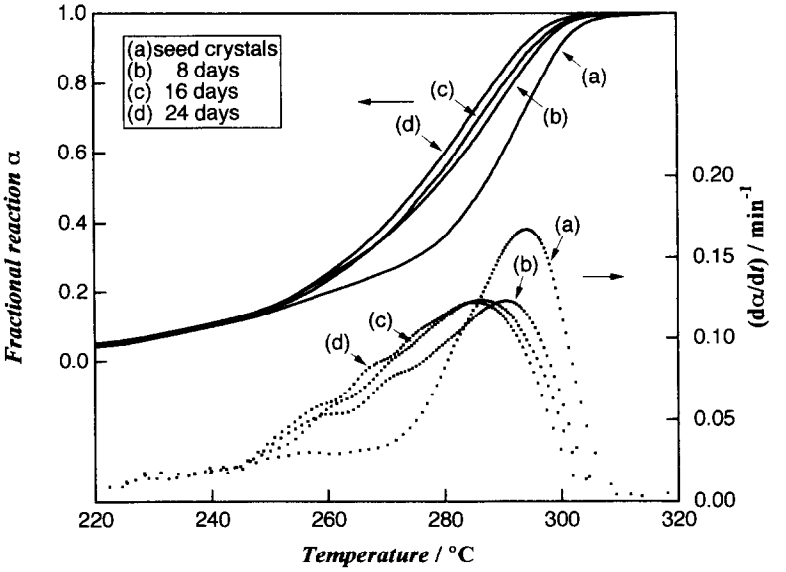

Fig. 4. Typical plots of α against T for the thermal decomposition of the samples after hydrothermal treatment, together with their derivative curves ($\phi = 5$ K min^{-1}).

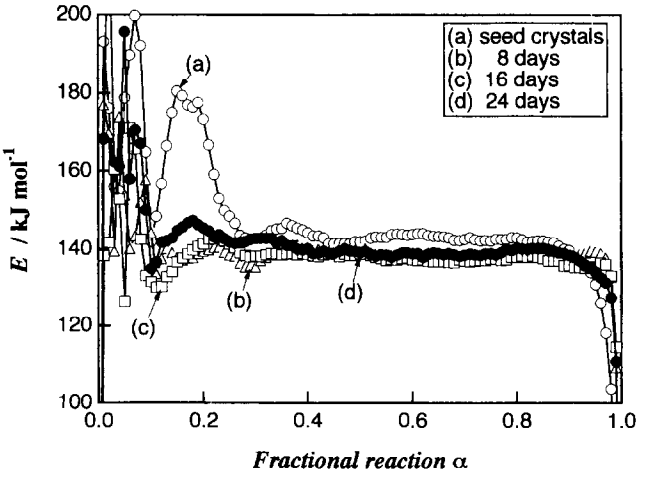

Fig. 5. The α dependence of the apparent values of E.

general kinetic equation [12]. The kinetic rate data were extrapolated to infinite temperature according to the equation [4, 13–16]

$$\frac{d\alpha}{d\theta} = \frac{d\alpha}{dt}\exp\left(\frac{E}{RT}\right) = Af(\alpha) \tag{2}$$

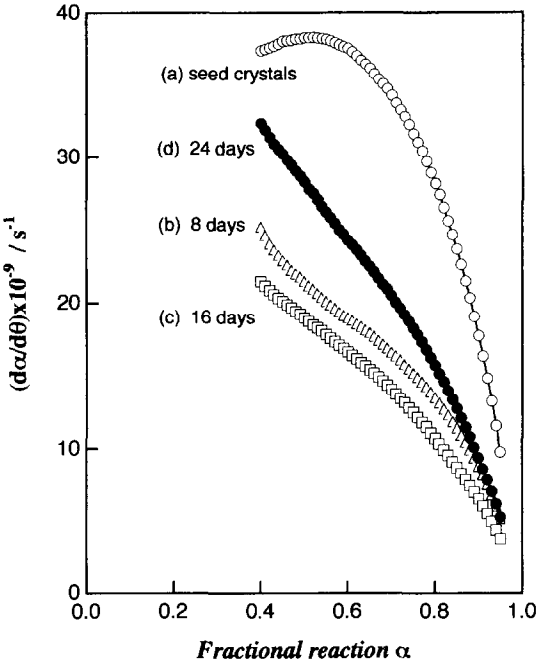

Fig. 6. The kinetic rate data extrapolated to infinite temperature.

where θ is the generalized time introduced by Ozawa [17, 18]. Fig. 6 shows the kinetic rate data at infinite temperature as plots of $d\alpha/d\theta$ against α. The kinetic rate data at infinite temperature for the smallest particle size, (a) seed crystals, exhibit the peak maximum at $\alpha_M = 0.52$. For the larger particle sizes, the rate data are predominantly deceleratory in the range $0.4 \leq \alpha \leq 0.95$.

In order to accomodate any deviation of the actual reaction mechanism from those assumed in deriving $f(\alpha)$ [3–6], the empirical kinetic model function $h(\alpha)$, expressed by multiplying $f(\alpha)$ by an accommodation function $a(\alpha)$: $h(\alpha) = f(\alpha)a(\alpha)$, was employed instead of $f(\alpha)$ in Eq. (2). The empirical kinetic model functions $h(\alpha)$ employed in the present study are of the type having nonintegral kinetic exponents in the original $f(\alpha)$, as listed elsewhere [1–6]. The most appropriate $h(\alpha)$ was estimated through plotting various $h(\alpha)$ against $d\alpha/d\theta$. Plots of the most appropriate $h(\alpha)$ against $d\alpha/d\theta$ are shown in Fig. 7. Table 1 summarizes the kinetic results including the averaged values of E, the most appropriate kinetic exponents in $h(\alpha)$, and the preexponential factor A calculated from the slope of the plots, together with the correlation coefficient of the linear regression analysis of the $h(\alpha)$ vs. $d\alpha/d\theta$ plot. The thermal decomposition kinetics of the smallest particle size was expressed by the A_M equation, $M(1-\alpha)[-\ln(1-\alpha)]^{1-1/M}$, indicating the nucleation and growth type mechanism. The correspondence to the R_N equation, $N(1-\alpha)^{1-1/N}$, observed for the larger particle size with exponents of about 2, implies two-dimensional shrinkage of the reaction interface.

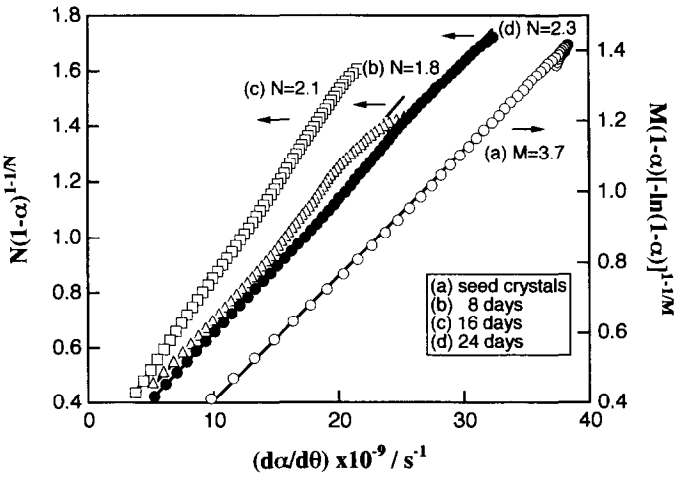

Fig. 7. The linear dependence of the most appropriate $h(\alpha)$ against $d\alpha/d\theta$.

Table 1
The kinetic results for the thermal decomposition of α-FeO(OH) after the hydrothermal treatment in a restricted range $0.4 \leq \alpha \leq 0.95$

Period of growth treatment/day	Mean value of E/kJ mol^{-1}	$h(\alpha)$	$A \times 10^{-10}$/s^{-1}	γ[a]
0	142.0 ± 0.6	$A_{3.7}$	2.816	0.9998
8	138.7 ± 0.2	$R_{1.8}$	1.928	0.9979
16	137.4 ± 0.2	$R_{2.1}$	1.502	0.9998
24	138.9 ± 0.2	$R_{2.3}$	2.039	0.9997

[a] Correlation coefficient for the linear regression analysis of the plots of $h(\alpha)$ against $d\alpha/d\theta$.

Because the A_M-type equation was originally derived for the nucleation and growth process under isothermal conditions, application of the A_M function for transformation under nonisothermal temperature change is not always acceptable [19]. The applicability of the A_M model for the present reaction of the smallest particle size is confirmed using the Sestak–Berrgren equation $SB(m, n)$ [20]: $h(\alpha) = \alpha^m(1-\alpha)^n$. The kinetic exponents m and n in the $SB(m, n)$ function are estimated using the following relationship [4, 14, 15]

$$\ln\left(\frac{d\alpha}{d\theta}\right) = \ln A + n \ln[\alpha^P(1-\alpha)] \quad \text{with} \quad P = \frac{m}{n} = \frac{\alpha_M}{1-\alpha_M} \tag{3}$$

The plot of $\ln(d\alpha/d\theta)$ against $\ln[\alpha^P(1-\alpha)]$ with $P = 1.08$ for the smallest particle size resulted in fairly good linearity with $\gamma = 0.9989$, from which the exponents $n = 0.82$ and $m = nP = 0.89$ were determined. Fig. 8 shows the correspondence of the experimental

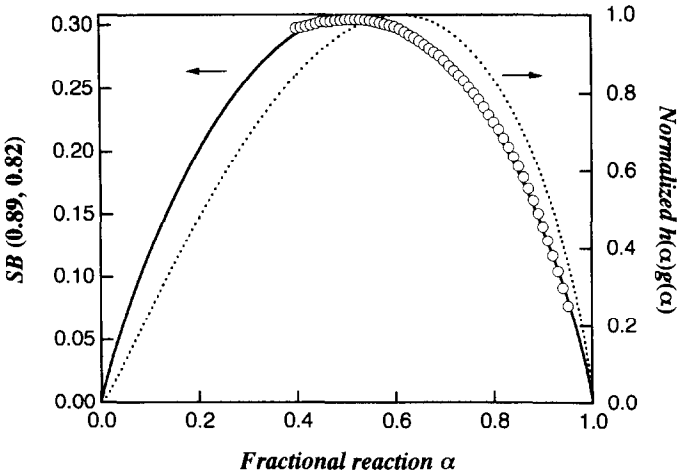

Fig. 8. Plots of $h(\alpha)$ and $h(\alpha)g(\alpha)$ against α according to the empirical SB (0.89, 0.82) function, together with the plot of experimental $d\alpha/A\,d\theta$ against α in the restricted range $0.4 \leq \alpha \leq 0.95$.

value of $d\alpha/A\,d\theta$ to the mathematically drawn $SB(0.89, 0.82)$ function. Within the restricted range $0.4 \leq \alpha \leq 0.95$, the rate data correspond perfectly to the $SB(0.89, 0.82)$ function with the standard deviation of the nonlinear regression analysis $\sigma = 0.0005$. The multiplication of function $h(\alpha)$ with its integral form $g(\alpha)$ can be used to distinguish the most appropriate kinetic model function [4, 14–16]. At infinite temperature, the function $h(\alpha)g(\alpha)$ is drawn by numerical integration of $h(\alpha)$ without assuming a constant heating rate during the reaction and approximation of the exponential integral [16]. A plot of $h(\alpha)g(\alpha)$ against α was drawn, numerically integrating the $SB(0.89, 0.82)$ function with respect to $0 \leq \alpha \leq 1$, as shown in Fig. 8. The function $h(\alpha)g(\alpha)$ reaches maximum at $\alpha_p^{\infty} = 0.61$, which corresponds very closely with the specific value of $\alpha_p^{\infty} = 0.632$ for the A_M functions. This implies that the A_M function is approximately applicable to the description of nonisothermal kinetics of the thermal decomposition of the smallest particle size.

The change in the appropriate kinetic model function from A_M-type to R_N-type with increasing particle size, indicates that surface nucleation is easier for the larger particles. This is consistent with the shift in the TG curves to the lower temperature region with increasing particle size, see Fig. 4. In interpreting the agreement to the A_M-type model for the smallest particle size, the overall kinetic result can be considered in connection with the distribution in the initiation temperature of the decomposition among the respective particles in the particle assemblage [21, 22]. Agreement with the R_N-type model for the grown particles seems to be interpreted on the basis of the respective particles. It is expected from the shift of the peak maxima in the derivative TG curves with increasing particle size and the higher transformation rate at infinite temperature for the largest particles compared with the other grown crystals, see Fig. 6, that the linear advancement rate of the reaction interface is larger for the crystals grown for

longer times. The crystal defects produced during the growth treatment are the most probable reason for this kinetic behavior.

4. Conclusion

In a buffer solution for Fe^{2+}, needle-liike crystals of α-FeO(OH) grow by air oxidation. The crystals contain irregular surface layers, which decompose thermally at a lower temperature than the original phase. During hydrothermal treatment, the irregular surface layers dissolve and form well-shaped crystals with smooth surfaces. The samples treated hydrothermally decompose thermally to α-Fe_2O_3 in a single step, as seen in the derivative TG curves. The nearly constant apparent activation energy of about 140 kJ mol^{-1} was obtained for the thermal decomposition in the restricted range $0.4 \leq \alpha \leq 0.95$, irrespective of the particle size of the samples. The thermal decomposition of the seed crystals treated hydrothermally gave the peak maxima of the decomposition rate extrapolated to infinite temperature at $\alpha = 0.52$ and showed good agreement with an A_M-type function with $M = 3.7$. The rate behavior of the grown crystals at infinite temperatue is predominantly deceleratory and agrees with R_N-type functions with $N \cong 2$. The switch in the appropriate kinetic model functions with the growth treatment time can be explained by the decrease in the particle size distribution and the higher reactivity of the grown layer compared to the original phase.

References

[1] N. Koga, S. Takemoto, S. Okada and H. Tanaka, Thermochim. Acta, 254 (1995) 193.
[2] N. Koga, S. Okada, T. Nakamura and H. Tanaka, Thermochim. Acta, 267 (1995) 195.
[3] J. Sestak, Thermophysical Properties of Solids, Elsevier, Amsterdam, 1984; J. Therm. Anal., 36 (1990) 36.
[4] N. Koga, J. Malek, J. Sestak and H. Tanaka, Netsu Sokutei, 20 (1993) 210.
[5] N. Koga and H. Tanaka, J. Therm. Anal., 41 (1994) 455.
[6] N. Koga and J. Malek, Thermochim. Acta, 282–3 (1996) 69.
[7] M. Kiyama, S. Shamoto, N. Horiishi, Y. Okuda and T. Takada, Bull. Inst. Chem. Res., Kyoto Univ., 64 (1986) 150.
[8] T. Asai, K. Ado and O. Nakamura, Chemistry Express, 6 (1991) 355 (in Japanese).
[9] A. Asai, K. Ado and O. Nakamura, Shikizai, 65 (1992) 68 (in Japanese).
[10] N. Koga and H. Tanaka, J. Phys. Chem., 98 (1994) 10521.
[11] H.L. Friedman, J. Polym. Sci., C6 (1964) 183.
[12] N. Koga, Thermochim. Acta, 224 (1994) 1.
[13] T. Ozawa, J. Therm. Anal., 2 (1970) 301.
[14] J. Malek, Thermochim. Acta, 200 (1992) 257.
[15] J. Sestak and J. Malek, Solid State Ionics, 63/65 (1993) 245.
[16] N. Koga, Thermochim. Acta, 258 (1995) 145.
[17] T. Ozawa, Bull. Chem. Soc. Jpn., 38 (1965) 1881.
[18] T. Ozawa, Thermochim. Acta, 100 (1986) 109.
[19] J. Malek, Thermochim. Acta, 267 (1995) 181.
[20] J. Sestak and G. Berrgren, Thermochim. Acta, 3 (1971) 1.
[21] H. Yoshioka, K. Amita and G. Hashizume, Netsu Sokutei, 11 (1984) 115 (in Japanese).
[22] Y. Masuda, K. Iwata, R. Ito and Y. Ito, J. Phys. Chem., 91 (1987) 6543.